Submitted for publication in ApJL
Preprint typeset using LaTeX style emulateapj v. 12/16/11

THE PLACE OF THE LOCAL GROUP IN THE COSMIC WEB

J. E. Forero-Romero[1] and R. González[2]
[1] Departamento de Física, Universidad de los Andes, Cra. 1 No. 18A-10, Edificio Ip, Bogotá, Colombia
[2] Instituto de Astrofsica, Pontificia Universidad Católica, Av. Vicuña Mackenna 4860, Santiago, Chile

Submitted for publication in ApJL

ABSTRACT

In this Letter we explore the characteristics of the Local Group (LG) location in the cosmic web using a cosmological simulation in the Λ CDM cosmology. We use a description for the cosmic web that uses the Hessian of the gravitational potential to classify a nieghborhodd in the simulation as either peak, sheet, filament or voids. We find that the LG pairs are preferentially located in filaments and sheets. Locally their locations are also located in a narrow range of overdensity $0 < \delta < 4$, ellipticity $0.1 < e < 1.0$ and prolateness $-0.5 < p < 0.5$. Furthermore we find a strong anti-alignment between the LG angular momentum vector and the filament lines and the sheet planes.

Subject headings: galaxies: Local Group — dark matter

1. INTRODUCTION

The configuration of galaxies in the Local Group (LG hereafter) is quite rare to find in the local Universe and in cosmological simulations. The LG is dominated by the two big spirals MW and M31, the next most-luminous galaxy is M33 which is $\sim$ 10 times less massive than M31, followed by several less luminous dwarf galaxies, up to a distance of $\sim$ 3Mpc. The velocity vector of M31, with a low tangential velocity is consistent to a head-on collision orbit toward the MW (Cox & Loeb 2008; van der Marel et al. 2012; Sohn et al. 2012).

Another feature of the Local group is the relatively low velocity dispersion of nearby galaxies up to ~ 8 Mpc (Sandage & Tammann 1975; Aragon-Calvo et al. 2011, and references therein). Environment around the Local Group has density quite close to the average density of the universe (Klypin et al. 2003; Karachentsev 2005). In addition, the closest massive galaxy cluster, the Virgo Cluster, is ≈ 16.5 Mpc away (Mei et al. 2007).

All this combination of features make LG analogues very rare to find. Using numerical simulatons González et al. (2013a) found less than 2% MW-sized halos reside in a pair similar to MW-M31 and in a similar environment. Furthermore, if we select pairs constrained within 2σ error fron current observational measurements of the velocity components and distance to M31, there are only 88 systems in a cube of 250 h^{-1}Mpc side.

Forero-Romero et al. (2013) also studied MW-M31 pairs in numerical simulations finding the typical quantities characterizing the orbital parameters of the LG are rare among typical pairs, but not enough to challenge the ΛCDM model. Another definition of LG analogues is made by Li & White (2008), but despite differences ocurr in the definitions and resulting fraction of LG analogues, all are in agreement with a low frequency of these pairs.

To better understand the properties of the LG and how this uncommon pair configuration fit in the cosmological context, an immediate question arise. What else can we say of the LG at larger scales?. In particular, which are the typical/prefered locations of these systems within the Cosmic Web?.

je.forero@uniandes.edu.co

Looking the LG at larger scales we have it is located in a difuse and warped filament/wall conecting Virgo Cluster with Fornax Cluster, some nearby galaxies and groups members of this large structure are the Maffei group, NGC 6744, NGC 5128, $M101$, $M81$, $NGC1023$, Cen A group. At this scale, there is no evident alignment of the MW-M31 orbital plane with the local filament or the Virgo-Fornax direction. However, if we look in a smaller volume below scales of $\sim$ 6 Mpc, there is a clear alignment of th the MW-M31 orbit with a local plane as shown by figure 3 in Courtois et al. (2013).

The environment definition we use in this Letter uses the tidal tensor field.

In this Letter we study the large scale environment of LG analogues in the context of ΛCDM. We use the Bolshoi simulation to explore in what structures they reside and if there is any correlation or alignment with the cosmic web. The large scale Environment is defined by the cosmic web components identified by Forero-Romero et al. (2009), and we use the LG analogues computed by González et al. (2013a). We pay spetial attention to quantify the kind of environment that hosts LG pairs and their alignments with respect to the prefered directions defined by the T-web.

This Letter is organized as follows. In Section 2 we present the N-body cosmological simulation and the algorithm to define the cosmic web, next in 3 we describe the sample of LG analogues extracted from the simulation. In Section 4 we presents our results to continue with a discussion about their implications for our Local Group in Section 5 to finally conclude in Section 6.

2. SIMULATION AND WEB FINDING ALGORITHM

2.1. *The Bolshoi simulation*

We use the Bolshoi simulation of ΛCDM cosmology: $\Omega_{\rm m} = 1 - \Omega_\Lambda = 0.27$, $H_0 = 70\,{\rm km/s/Mpc}$, $\sigma_8 = 0.82$, $n_s = 0.95$ (Klypin et al. 2011), compatible with the constraints from the WMAP satellite (Hinshaw et al. 2013). The simulation followed evolution of dark matter in a $250h^{-1}$Mpc box with spatial resolution of $\approx 1h^{-1}$ kpc

and mass resolution of $m_{\rm p} = 1.35 \times 10^8$ M$_\odot$. Halos are identified with the BDM algorithm (Klypin & Holtzman 1997). The BDM algorithm is a spherical overdensity halo finding algorithm and is designed to identify both host halos and subhalos.

2.2. *Cosmic web identification*

The web finding algorithm is based on the tidal tensor computed as the Hessian of the gravitational potential field

$$T_{ij} = \frac{\partial^2 \phi}{\partial r_i \partial r_j}, \quad (1)$$

where r_i, $i = 1, 2, 3$ refers to the three spatial comoving coordiates and ϕ is the gravitational potential renormalized to follow the following Poisson equation $\nabla^2 \phi = \delta$ where δ is the matter overdensity.

This tensor is real and symmetric, which means that can be diagonalized. We note its eigenvalues as $\lambda_1 \geq \lambda_2 \geq \lambda_3$ and their corresponding eigenvectors $\hat{e}_1$, $\hat{e}_2$ and $\hat{e}_3$. The web classification compares each one of the three eigenvalues to a threshold value $\lambda_{\rm th}$. If the three, two, one or zero eigenvalues are larger than this threshold the region is classified as peak, filament, sheet or void, respectively.

Forero-Romero et al. (2009) performed a detailed study for the topology of the cosmic web and its visual counterpart as a function of the parameter $\lambda_{\rm th}$. They found that reasonable results in terms of the volume fraction occupied by voids, the visual inspection and the halo populations in each web type can be reached by values of $0.2 < \lambda_{\rm th} < 0.4$. In this Letter we choose the value of $\lambda_{\rm th} = 0.3$ to proceed with our analysis. We have veryfied that the main trends reported in this paper are unsensitive to the choice of that parameter, as long as it is in the range already quoted.

The algorithm to compute the potential is grid based. First we interpolate the density into a cubic grid with a Cloud-In-Cell (CIC) scheme and smooth it with a gaussian kernel. Then we obtain the gravitational potential using FFT methods and use finite differences to compute the Hessian at every point in the grid. In our case we have used a grid size on and a gaussian smoothing with two times larger as the typical separation between the two halos in the Local Group. The purpose of this choice is to have both halos in the pair a common environment. In this paper we use a grid spacing of $s = 0.97$ h^{-1}Mpc , corresponding to a 256^3 grid in the Bolshoi volume. The scale for the gaussian smoothing uses the same value.

After computing the eigenvalues and eigenvectors on each point of the grid we use the matter overdensity, ellipticity and the prolatenes to further characterize the web. These quantities are defined in terms of the eigenvalues as follows

$$\delta = \lambda_1 + \lambda_2 + \lambda_3, \quad (2)$$

$$e = \frac{\lambda_3 - \lambda_1}{2(\lambda_1 + \lambda_2 + \lambda_3)}, \quad (3)$$

$$p = \frac{\lambda_1 + \lambda_3 - 2\lambda_2}{2(\lambda_1 + \lambda_2 + \lambda_3)}. \quad (4)$$

We are also interested in measuring the alignment of the LG halos with respect to the cosmic web. To this end we characterize each LG pair by the vector that is normal to the orbital plane, which is defined by the position and velocities of each halo with respect to the center of mass.

3. LOCAL GROUP ANALOGUES

To construct a sample of the MW-M31 pairs at $z \approx 0$, we use a series of simulation snapshots at $z < 0.1$ (i.e. in the last ≈ 1.3 Gyr before present) spaced by $\approx 150 - 250$ Myr. This is done because a particular configuration of MW and M31 is transient and corresponds to a relatively small number of systems at one snapshot. By using multiple snapshots we can increase the sample of systems in such configuration during a period of time in which secular cosmological evolution is small.

Pairs are selected allowing a wide range of masses, following an isolation critera, constraining by orbital measurements such as radial, tangential velocity and separation of the pair, and local environment constrains such as local velocity dispersion and local overdensity within a sphere of radius 5 Mpc. A full description of the selection criteria can be found in González et al. (2013a,b).

We define two samples according to the tolerance in the selection constraints: A sample named 2σ, correspondig to LG analogues constrained by two times the observational errors in the orbital values (radial velocity, tangential velocity, and separation), and a more relaxed sample named 3σ for LG analogues constrained by three times observational errors accordingly. The number of pairs in each sample is 46 and 120 respectively, notice we have less pairs than in González et al. (2013a) results, since we removed pairs which are too close at $z = 0$, i.e. their virial radii overlaps, also we removed a couple pairs that merged or change their mass more than 20% at present time since they were detected at $z < 0.1$.

We also have a third general sample that we use as a control for our results. **What are the criteria for this sample?**

4. RESULTS

4.1. *The prefered environment for LGs*

The first result we explore is the kind of environment occupied by our LGs. We find that the LGs in the general sample are located across all different evironment without any strong preferences; 1/3 are located in sheets, 1/4 in peaks, 1/4 in filaments and the remaning 1/6 in voids.

The situation in the restricted 2σ and 3σ samples is very different. By large the LGs in these samples are located in filaments and sheets. In both samples, $\sim 50\%$ of the pairs can be found in filaments while $\sim 40\%$ are in in sheets. These absolute numbers in each environment for each sample are presented in Table 1.

4.2. *Alignment along the cosmic web*

We now explore the alignment of the pairs with respect to the cosmic web. First we define the unit vector $\hat{r}$ that links the two halos. Then, we compute the dot product of $\hat{r}$ and each one of the three eigenvectors for pair in the three samples. In Figure 1 we show the main result of that study, it presents the cumulative distribution of $\mu \equiv \hat{e}_3 \cdot \hat{r}$ for pairs located in filaments and sheets. The straight line corresponds to the expected result for a random vector distribution.

Sample	Peak	Filament	Sheet	Void
	n (%)	n (%)	n (%)	n (%)
2σ	4 (8.7)	24 (52.2)	17 (36.7)	1 (2.2)
3σ	10 (8.3)	58 (48.3)	47 (39.2)	5 (4.2)
General ($12.1 < \log_{10} M_{\rm h}/{\rm M}_\odot < 12.3$)	8 (1.4)	334 (55.5)	259 (43.0)	1 (0.1)

TABLE 1
Number of pairs in the four different kinds of environments. In parethesis the same number as a percentage of the total population.

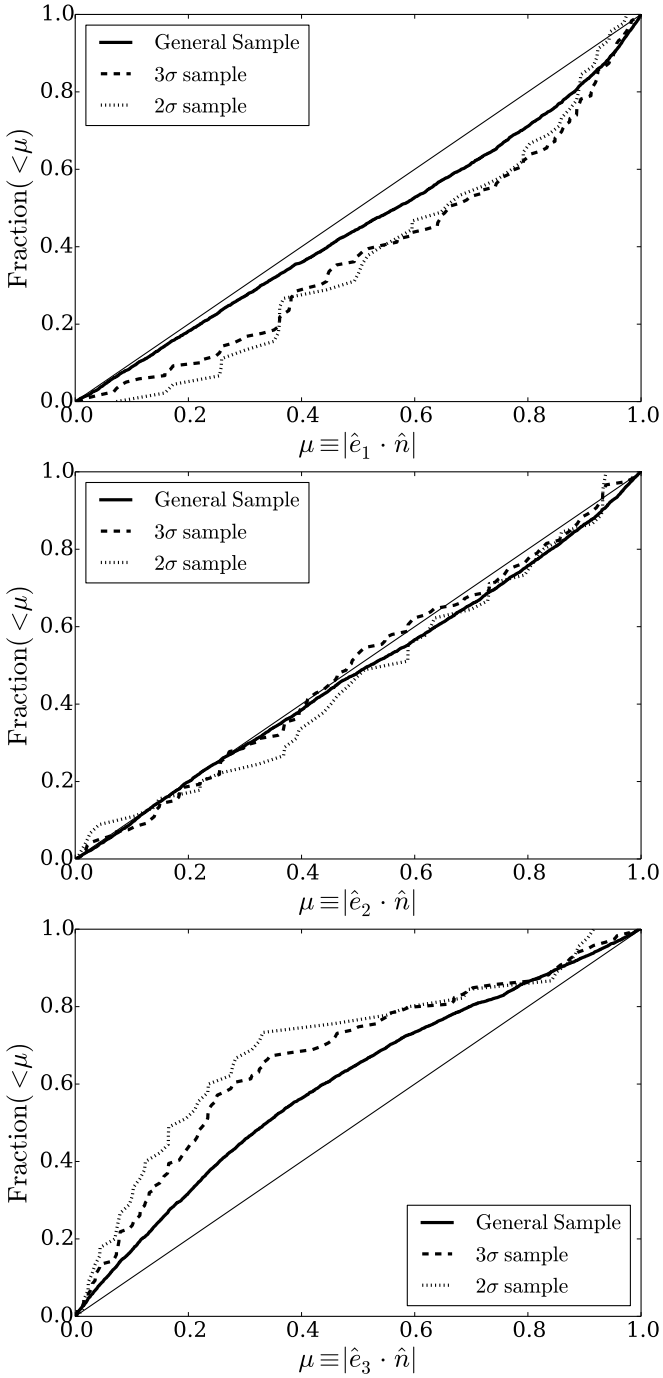

Fig. 1.— Cumulative distributions for the alignment between the normal vector $\hat{n}$, and the eigenvectors defining the cosmic web.

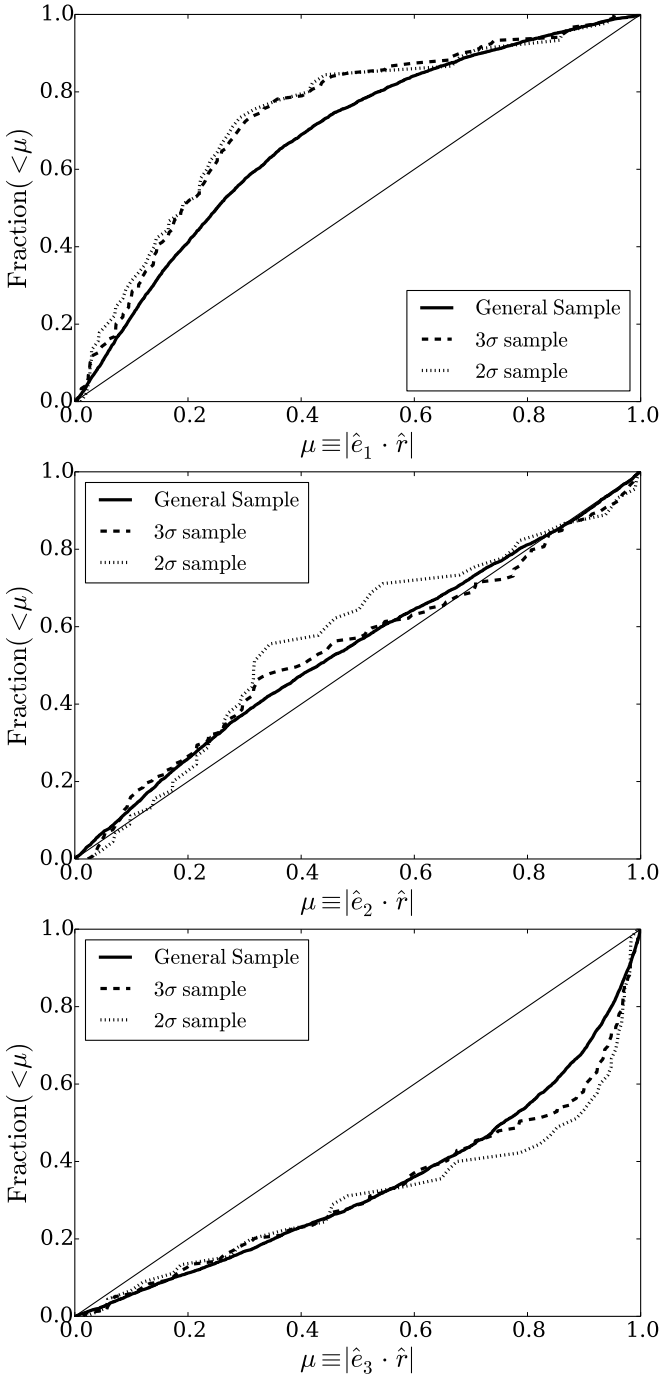

Fig. 2.— Cumulative distributions for the alignment between the unit vector linking the two halos, $\hat{r}$, and the eigenvectors defining the cosmic web.

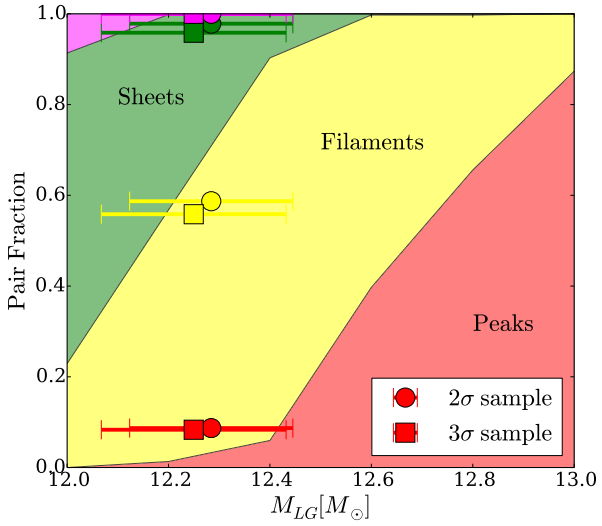

FIG. 3.— Mass dependency of the fraction of pairs in the different environemnts.

From this Figure we first see that there is a clear distinct behavior between the general samples and the 3σ-2σ samples. The general sample tenst to be aligned along the $\hat{e}_3$ vector, the 3σ sample does not show any strong alignment and the 2σ pairs tend to be perpendicular to the $\hat{e}_3$ vector and slightly parallel to $\hat{e}_1$. These trends hold in filaments and walls.

Let's focus on filaments first. That result means that in the general sample the two halos tend to lie along the filament, while in the 2σ-3σ samples they are located perpendicular to the filament. If one considers that in these samples the motion is radial, that means that the pairs are moving into the filament.

In the case of sheets, the pairs in the general sample tend to lie on the sheet plane along the direction of the slowest collapsing direction. In the 2σ samples the pairs are not constrained to the plane anymore and are perpendiculat to the $\hat{e}_3$ vector. Considering the preferential radial motion of these pairs, that mens that the pairs are moving into the pancake all over a plane that is itself perpendicular to the sheet.

4.3. *Overdensity, Ellipticity and Anisotropy*

We now describe the preferred place of the LG samples in terms of the overdensity, ellipticiy and anisotropy as defined in Section 2.

Figure **??** shows that the range of overdensities for the general pair sample spans almost two orders of magnitude from underdense regions $\delta < 0$ to high density regions $\delta \sim 30$, with a distribution peaking around $\delta \sim 0$. In contrast the 2σ and 3σ samples are located within a narrower range of overdensities $0.0 < \delta < 4.0$ peaking at $\delta \sim 1.5$. This is consistent with the fact that these samples are mostly found in filaments and sheets.

Figure **??** presents the cumulative distribution for the ellipticity and prolateness. The general sample presents a wide range in ellipticity that can range from $-30 < e < 30$. For the 2σ and 3σ samples most of the pairs are now located in a narrow range for ellipticities in the range $0.1 < e < 1.0$. This condition on the ellipticity together with the fact that $\delta > 0$ implies that the prolateness in these samples must be bounded by $-1.0 < p < 1.0$. We actually find that they most of the pairs are bounded to an even narrower range $0.5 < p < 0.5$.

Figure **??** shows two panels with the joint scatter plot for the ellipticity and the prolateness as a function of the overdensity. For clarity we only include the general and 3σ samples. In the left panel (ellipticity) we see the a simple cut in the overdensity is not enough to explain the narrow ranges in the ellipticity; the LG pairs in the 3σ sample are located towards low ellipticity values. In the right panel (prolateness) we find a similar situation; a cut in the overdensity would produced a wider distribution in prolateness values than the one featured by the 3σ sample.

5. DISCUSSION

6. CONCLUSIONS

ACKNOWLEDGEMENTS

REFERENCES

Aragon-Calvo, M. A., Silk, J., & Szalay, A. S. 2011, MNRAS, 415, L16
Courtois, H. M., Pomarède, D., Tully, R. B., Hoffman, Y., & Courtois, D. 2013, AJ, 146, 69
Cox, T. J., & Loeb, A. 2008, MNRAS, 386, 461
Forero-Romero, J. E., Contreras, S., & Padilla, N. 2014, ArXiv e-prints
Forero-Romero, J. E., Hoffman, Y., Bustamante, S., Gottlöber, S., & Yepes, G. 2013, ApJ, 767, L5
Forero-Romero, J. E., Hoffman, Y., Gottlöber, S., Klypin, A., & Yepes, G. 2009, MNRAS, 396, 1815
González, R. E., Kravtsov, A. V., & Gnedin, N. Y. 2013a, ArXiv e-prints
—. 2013b, ApJ, 770, 96
Hinshaw, G., Larson, D., Komatsu, E., Spergel, D. N., Bennett, C. L., Dunkley, J., Nolta, M. R., Halpern, M., Hill, R. S., Odegard, N., Page, L., Smith, K. M., Weiland, J. L., Gold, B., Jarosik, N., Kogut, A., Limon, M., Meyer, S. S., Tucker, G. S., Wollack, E., & Wright, E. L. 2013, ApJS, 208, 19
Karachentsev, I. D. 2005, AJ, 129, 178
Klypin, A., Hoffman, Y., Kravtsov, A. V., & Gottlöber, S. 2003, ApJ, 596, 19
Klypin, A., & Holtzman, J. 1997, ArXiv Astrophysics e-prints
Klypin, A. A., Trujillo-Gomez, S., & Primack, J. 2011, ApJ, 740, 102
Li, Y.-S., & White, S. D. M. 2008, MNRAS, 384, 1459
Mei, S., Blakeslee, J. P., Côté, P., Tonry, J. L., West, M. J., Ferrarese, L., Jordán, A., Peng, E. W., Anthony, A., & Merritt, D. 2007, ApJ, 655, 144
Sandage, A., & Tammann, G. A. 1975, ApJ, 196, 313
Sohn, S. T., Anderson, J., & van der Marel, R. P. 2012, ApJ, 753, 7
van der Marel, R. P., Fardal, M., Besla, G., Beaton, R. L., Sohn, S. T., Anderson, J., Brown, T., & Guhathakurta, P. 2012, ApJ, 753, 8

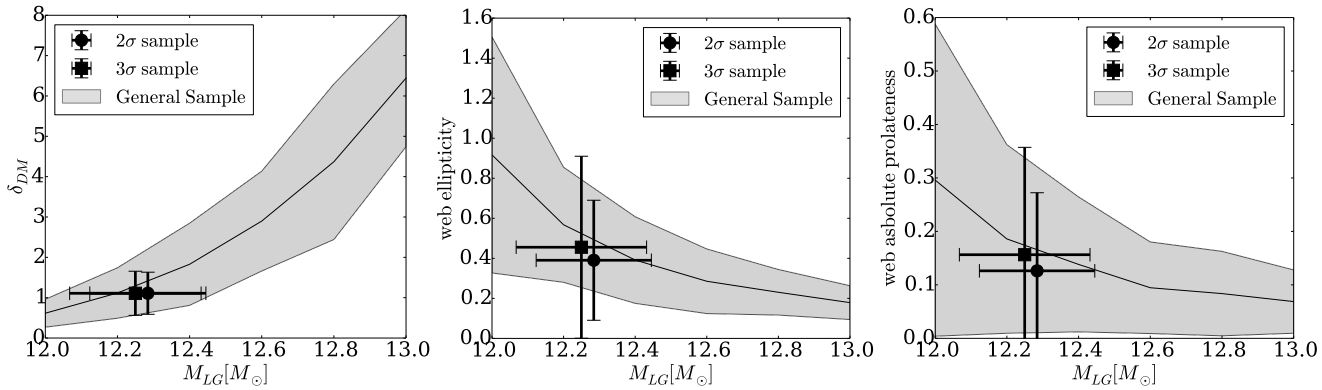

FIG. 4.— Mass dependency of the average dark matter overdensity (left), web ellipticity (middle) and web absolute value prolateness (right) at the pair location.

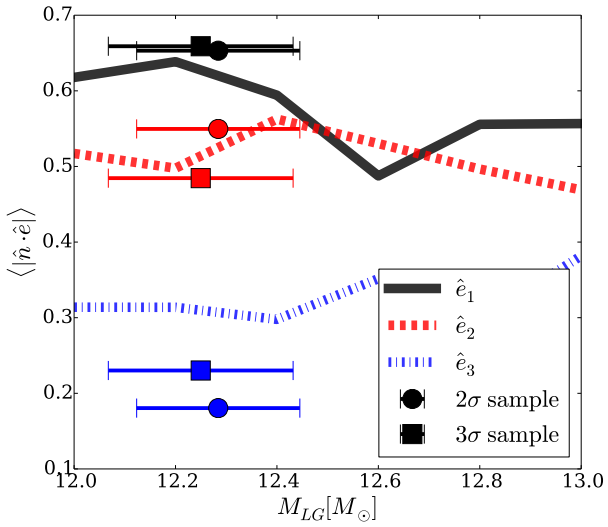

FIG. 5.— Mass dependency of the median value for the dot product between the normal vector $\hat{n}$ and each one of the eigenvectors. The lines show the trends for the general sample.

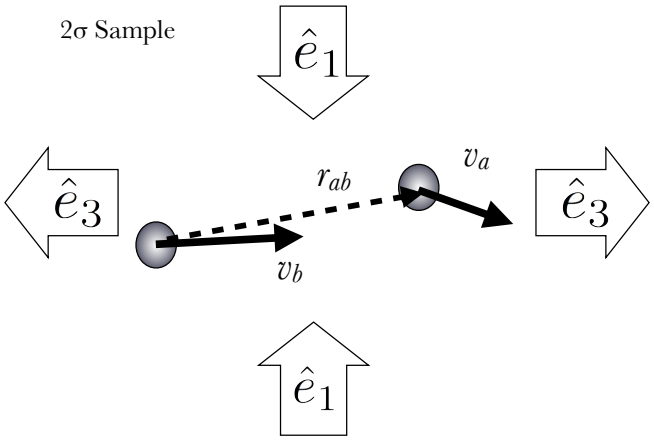

FIG. 6.— Schematic picture of the strongest alignment tendencies in the the General and 2σ-3σ samples. The alignment between the peculiar velocities and the $\hat{e}_3$ eigenvector was reported in Forero-Romero et al. (2014) for all halos regardles of its mass. 1.

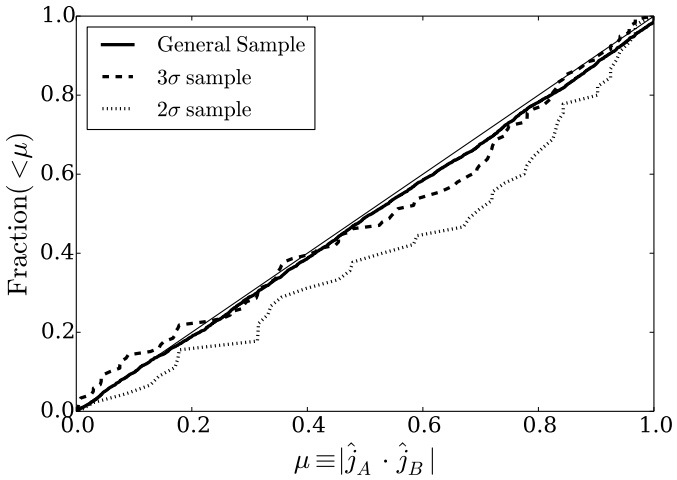

FIG. 7.— Alignment between the two angular momentum vectors of the two halos in the pair.